Check for updates

Sequential detection of hypochlorous acid and sulfur dioxide derivatives by a red-emitting fluorescent probe and bioimaging applications *in vitro* and *in vivo*†

Jianhua Liu,‡[ac] Haoyuan Yin,‡[a] Zhuye Shang,[a] Pengli Gu,[b] Guangjie He,*[b] Qingtao Meng, [iD] *[a] Run Zhang [iD] [d] and Zhiqiang Zhang*[a]

Hypochlorous acid (HOCl) and sulfur dioxide derivatives (SO_3^{2-}/HSO_3^{-}) play critical roles in complex signal transduction and oxidation pathways. Therefore, it is meaningful and valuable to detect both HOCl and SO_2 derivatives in biosystems by a fluorescence imaging assay. In this work, we developed a red-emitting fluorescent probe (DP) by the condensation of malononitrile and phenothiazine derivatives through a C=C double bond. DP was designed with a donor−π−acceptor (D−π−A) structure, which enables absorption and emission in the long wavelength region. In the presence of HOCl, specific oxidation of the thioether of phenothiazine in DP to a sulfoxide derivative (DP=O) occurs, resulting in a hypochromic shift (572 nm to 482 nm) of the absorption spectra and "OFF−ON" response of the maximum emission at 608 nm. After the activation of the C=C double bond by oxidation, DP=O reacts specifically with SO_3^{2-}/HSO_3^{-} *via* a 1,4-nucleophilic addition reaction leading to a decrease in the intensity of the absorption and emission spectra, which enabled the realization of sequential detection of HOCl and SO_3^{2-}/HSO_3^{-} by a single fluorescent probe. The detection limits of DP for HOCl and SO_3^{2-}/HSO_3^{-} were calculated to be 81.3 nM and 70.8 nM/65.1 nm, respectively. The results of fluorescence microscopic imaging indicated that DP shows potential for the detection of intracellular HOCl and SO_3^{2-}/HSO_3^{-}. Using adult zebrafish and nude mice as live animal models, DP was successfully used for the fluorescence imaging of HOCl and SO_3^{2-}/HSO_3^{-} *in vivo*.

Introduction

Reactive oxygen species (ROS), including mainly HOCl, H_2O_2, HO, and O_2^{-}, play crucial roles in various regular biochemical approaches and irregular pathological pathways.[1–3] Among the ROS, hypochlorous acid (HOCl) and the dissociated hypochlorite ion (OCl^{-}) are strong oxidants found in human bodies while being widely used in our daily life as a bleach.[4–6] Endogenous HOCl is usually generated from hydrogen peroxide and chloride ions by secreted myeloperoxidase (MPO) *in vivo* in response to inflammatory stimuli.[7,8] The physiologically relevant levels of HOCl in living organisms are 5–25 μM.[9] It has been evidenced that excessively generated HOCl is related to extensive oxidative stress and oxidative damage, leading to numerous diseases such as neurodegeneration including Parkinson's disease and Alzheimer's disease, inflammatory diseases, atherosclerosis and cancer.[10–14]

Cells often possess an elaborate antioxidant defense system to regulate their internal redox equilibrium.[15–17] Sulfur dioxide (SO_2), one of the reactive sulfur species (RSS), participates actively in equilibrating the redox status as an antioxidant against ROS.[18–20] SO_2 forms two reductive derivatives: sulfite (SO_3^{2-}) and bisulfite (HSO_3^{-}) (3 : 1 M/M, in neutral fluids).[21,22] It is believed that SO_2 derivatives play crucial roles in a wide range of physiological and pathological processes such as vaso-relaxant, antihypertensive, antiatherogenic, and antioxidative effects.[23–25] However, excessive intake of SO_3^{2-}/HSO_3^{-} is associated with a variety of adverse effects and acute symptoms such as flushing, hypotension, diarrhea, urticaria, and abdominal pain.[26–29] In addition, excessive intake of HSO_3^{-} can lead to a variety of diseases such as cancer, nervous system disorders, asthma and allergic reactions, and even tissue damage.[30] Food

[a]School of Chemical Engineering, University of Science and Technology Liaoning, Anshan, Liaoning Province, 114051, P. R. China. E-mail: qtmeng@ustl.edu.cn; zzq@ustl.edu.cn; Tel: +86-412-5929627

[b]School of Forensic Medicine, Xinxiang Medical University, Jinsui Road No. 601, Xinxiang, Henan Province, 453003, P. R. China. E-mail: guangjiehe@163.com

[c]College of Pharmacy, Jilin Medical University, Jilin Province, 132001, P. R. China

[d]Australian Institute for Bioengineering and Nanotechnology, The University of Queensland, Brisbane, 4072, Australia

and Agriculture Organization (FAO) and World Health Organization (WHO) have recommended that the daily intake of sulfites/bisulfites per person be less than 0.7 mg kg^{-1} (body weight) in view of the serious health risks associated with excessive intake of HSO_3^-.[31] In view of the important roles of ROS/RSS-regulated redox homeostasis in biosystems, it is meaningful and valuable to develop efficient methods for monitoring $HOCl/SO_2$ derivatives regulating redox cycle processes *in vitro* and *in vivo*, which is vital for biological research as well as clinical diagnoses.

Among the various bioanalytical methods, fluorescence imaging technology has been regarded as a powerful visual methodology for the detection and monitoring of various biological components due to its advantages such as high sensitivity, good selectivity, little invasiveness and real-time detection.[32–35] To date, number of fluorescent probes have been designed and reported for the individual detection and visualization of HOCl and SO_3^{2-}/HSO_3^- in biosystems and real water or food samples.[36–46] However, a fluorescent probe specifically for detecting and monitoring both HOCl and SO_2 derivatives in biosystems and visually detecting SO_2 derivatives in real samples is rarely reported.[47,48] Herein, we developed a red-emitting fluorescent probe (**DP**) by linking malononitrile and phenothiazine derivatives through a C=C double bond. In the presence of HOCl, specific oxidation of the thioether of **DP** to a sulfoxide derivative (**DP=O**) occurs, resulting in a hypochromic shift (574 nm to 480 nm) of the absorption spectra and "OFF–ON" response of the emission. After the activation of the C=C double bond by oxidation, the oxidation product (**DP=O**) reacts with SO_3^{2-}/HSO_3^- *via* a 1,4-nucleophilic addition reaction leading to a decrease in the intensity of the absorption and emission spectra, which enabled the realization of sequential detection of HOCl and SO_3^{2-}/HSO_3^- by a single fluorescent probe (Scheme 1).

Results and discussion

Design, synthesis and characterizations of fluorescent probe (DP)

The probe **DP** was synthesized *via* a one-step condensation reaction between 2-[3-cyano-4,5,5-trimethylfuran-2(5H)-ylidene]malononitrile (DCDHF) and 10-ethyl-10H-phenothiazine-3-carbaldehyde in the presence of catalytic amounts of piperidine in methanol (Scheme S1†). The chemical structure of **DP** was characterized by ^1H NMR, ^{13}C NMR and HRMS (Fig. S1–S3†). **DP** was designed with a donor–π–acceptor (D–π–A) structure, in which a phenothiazine unit acts as an electron-donating group (EDG), while DCDHF acts as an electron-

withdrawing group (EWG). The large π-conjugation structure enables **DP** to absorb and emit in the long wavelength region. **DP** features outstanding water solubility, allowing its application in 90% PBS aqueous solutions (DMF : H_2O = 1 : 9, v/v, 20 mM, pH = 7.4). In addition, only small fluctuations in the fluorescence intensity of **DP** at 608 nm were found within 30 h in the HEPES aqueous buffer (Fig. S4†), suggesting the high stability of **DP** under simulated physiological conditions. The proposed reaction mechanisms of **DP** towards HOCl and SO_3^{2-}/HSO_3^- were first studied by HR MS titration measurement. As shown in Fig. S5,† after addition of HOCl, the molecular ion peak assigned to **DP** at 451.15936 ([**DP+H**]$^+$, m/z, calcd.: 451.15926) disappeared and a new peak belonging to the oxidized sulfoxide product (**DP=O**) emerged at m/z 467.1558 ([**DP=O+H**]$^+$, m/z, calcd. 467.1536). Sequentially, upon the addition of HSO_3^- to the solution of **DP=O**, a new peak assigned to the addition product **DP=O–SO$_3$** ([**DP=O–SO$_3$**]$^-$, m/z, calcd. 547.1115) emerged at m/z 547.1191 (Fig. S6†). Similarly, a new peak assigned to the addition product **DP=O–SO$_3$** also appeared at m/z 547.1135 in the presence of SO_3^{2-} (Fig. S7†).

Spectroscopic responses of DP towards HOCl

With probe **DP** in hand, we first tested the spectroscopic response of **DP** (10 μM) in stimulated physiological media (PBS : H_2O = 1 : 9, v/v, 20 mM, pH = 7.4). In PBS aqueous solutions, **DP** displayed a main absorption band centered at 574 nm. Upon the addition of various analytes such as reactive oxygen species (HOCl, H_2O_2, $^1O_2$, $ONOO^-$, $OH^{\cdot}$ and O_2^-), reactive sulfur species (Cys, GSH, Hcy, S^{2-}, SO_3^{2-}, HSO_3^-, HSO_4^- and SO_4^{2-}) and biologically relevant anions (Br^-, F^-, Cl^-, $P_2O_7^{4-}$, PO_4^{3-}, $H_2PO_4^-$, OH^-, CH_3COO^-, HCO_3^-, NO_3^- and NO_2^-) to the solution of **DP**, only HOCl contributed to the major absorption peak of **DP** at 574 nm, which gradually decreased accompanied by a new absorption peak appearing at 480 nm. Significant changes were not observed in the absorption spectra upon the addition of the aforementioned competitive species (Fig. 1A). The absorption spectra response of **DP** towards HOCl was then investigated by a titration experiment. As presented in Fig. 1B, upon the addition of increasing amounts of HOCl (0–60 μM), the major peak of **DP** centered at 574 declined notably and an intense absorption band centred at 480 nm appeared and enhanced gradually. The new absorption was attributed to the HOCl-induced oxidation product (**DP=O**). The absorbance ratio ($A_{480 nm}/A_{574 nm}$) of **DP** became constant and the blue solution of **DP** turned to yellowish-brown when the concentration of HOCl reached 50 μM (Fig. 1B, inset). Furthermore, two clear isosbestic points at 426 nm and 525 nm emerged in the presence of HOCl, which indicated the quantitative reaction of **DP** with HOCl. The specificity of **DP** toward HOCl was then validated by a "naked-eye" colorimetric assay. As shown in Fig. 1C, the color of the **DP** solution was changed from blue to yellowish-brown specifically in the presence of HOCl, suggesting that **DP** can serve as a potential "naked-eye" indicator for HOCl detection.

The sensing behavior of **DP** toward various analytes was further tested with fluorescence spectra. The solution of free **DP**

Scheme 1 Proposed sensing mechanism of DP for the sequential detection of HOCl and SO_2 derivatives (SO_3^{2-}/HSO_3^-).
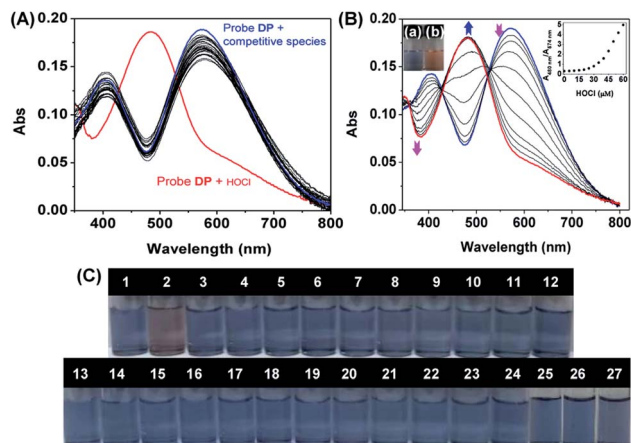
Fig. 1 (A) Absorption spectra of probe **DP** (10 μM) in PBS aqueous solutions (DMF : H₂O = 1 : 9, v/v, 20 mM, pH = 7.4) upon addition of various analytes (60 μM). (B) UV-vis absorption spectra of probe **DP** (10 μM) in the presence of different amounts of HOCl (0–60 μM) in PBS aqueous solutions (DMF : H₂O = 1 : 9, v/v, 20 mM, pH = 7.4). Inset: absorbance ratio of probe **DP** at 480 nm and 574 nm as a function of HOCl concentration. Colorimetric changes of probe **DP** (a) in the absence and (b) in the presence of HOCl (60 μM). (C) Colorimetric changes of probe **DP** (10 μM) in the presence of various analytes (60 μM): (1) free **DP**, (2) HOCl, (3) Br⁻, (4) F⁻, (5) Cl⁻, (6) P₂O₇⁴⁻, (7) PO₄³⁻, (8) H₂PO₄⁻, (9) Cys, (10) GSH, (11) Hcy, (12) S²⁻, (13) SO₃²⁻, (14) HSO₃⁻, (15) H₂O₂, (16) ¹O₂, (17) OH⁻, (18) CH₃COO⁻, (19) HCO₃⁻, (20) NO₃⁻, (21) ONOO⁻, (22) NO₂⁻, (23) NO₃⁻, (24) HSO₄⁻, (25) SO₄²⁻, (26) OH˙ and (27) O₂⁻.

shows no fluorescence emission in PBS aqueous solutions (DMF : H₂O = 1 : 9, v/v, 20 mM, pH = 7.4). Subsequently, upon increasing the amount of HOCl (0–60 μM), the fluorescence emission band at 608 nm increased dramatically with excitation at 480 nm (Fig. 2A). The fluorescence intensity of **DP** reached platform until the concentration of HOCl reached 5.0 equiv., resulting in a fluorescence color change from colourless to red (Fig. 2A(a and b)). To further understand the fluorescence enhancement mechanism of **DP** in the presence of HOCl, density functional theory (DFT) calculations were performed using Materials Studio 2019 (Fig. S8, Tables S1 and S2†). The optimized molecular frontier orbital distribution and corresponding electric energies of **DP** and **DP═O** are presented in Fig. S8.† The highest occupied molecular orbit (HOMO) of **DP** is mainly localized to the phenothiazine moiety, while the lowest unoccupied molecular orbital (LUMO) is primarily localized to the malononitrile (DCDHF) unit. Thus, an intra-molecular charge transfer (ICT) took place through the C═C conjugated bridge from phenothiazine to the DCDHF moiety, which results in a silent fluorescence emission of **DP**.[49] However, after HOCl-triggered oxidation of the thioether of phenothiazine to the sulfoxide unit, the HOMO of **DP═O** is distributed throughout the molecule of **DP═O**. As a result, the ICT-induced quenching effect is inhibited, resulting in the enhancement of the fluorescence emission.[50]

The fluorescence emission increase of **DP** at 608 nm showed a good linear relationship with the concentration of HOCl (3.2–35 μM) (Fig. 2A(c)), and the detection of limit was calculated to
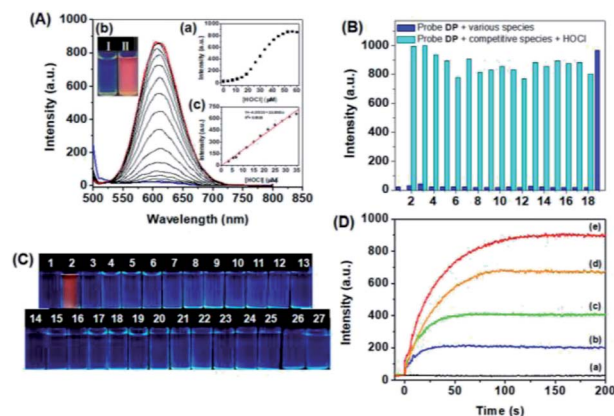

Fig. 2 (A) Fluorescence spectra of probe **DP** (10 μM) in the presence of different amounts of HOCl (0–60 μM) in PBS aqueous solutions (DMF : H₂O = 1 : 9, v/v, 20 mM, pH = 7.4). Inset: (a) fluorescence intensities of probe **DP** at 608 nm as a function of HOCl concentration. (b) Fluorescence color changes of probe **DP** (I) in the absence and (II) in the presence of HOCl. (c) Linear relationship between the fluorescence intensity of **DP** (5 μM) at 608 nm and HOCl concentration (3.2–35 μM). (B) Changes in the fluorescence intensity of probe **DP** (10 μM) towards HOCl (60 μM) in the presence of various competing analytes (60 μM): (1) blank, (2). Br⁻, (3) F⁻, (4) Cl⁻, (5) P₂O₇⁴⁻, (6) PO₄³⁻, (7) H₂PO₄⁻, (8) ¹O₂, (9) OH⁻, (10) CH₃COO⁻, (11) HCO₃⁻, (12) NO₃⁻, (13) ONOO⁻, (14) NO₂⁻, (15) HSO₄⁻, (16) SO₄²⁻, (17) OH˙, (18) O₂⁻, (19) HOCl. (C) Fluorescence colour images of probe **DP** (10 μM) in the presence of various analytes (60 μM) under UV light of 365 nm. (1) Free **DP**. (2) HOCl. (3) Br⁻, (4) F⁻, (5) Cl⁻, (6) P₂O₇⁴⁻, (7) PO₄³⁻, (8) H₂PO₄⁻, (9) Cys, (10) GSH, (11) Hcy, (12) S²⁻, (13) SO₃²⁻, (14) HSO₃⁻, (15) H₂O₂, (16) ¹O₂, (17) OH⁻, (18) CH₃COO⁻, (19) HCO₃⁻, (20) NO₃⁻, (21) ONOO⁻, (22) NO₂⁻, (23) NO₃⁻, (24) HSO₄⁻, (25) SO₄²⁻, (26) OH˙ and (27) O₂⁻. (D) Time-profile fluorescence enhancement at 608 nm of probe **DP** in the presence of (a) 0 μM, (b) 20 μM, (c) 25 μM, (d) 35 μM and (e) 50 μM HOCl in PBS aqueous solutions. Excitation was performed at 480 nm.

be 81.3 nM according to the reported method defined by IUPAC.[51] Then, the selectivity of **DP** toward various analytes was evaluated. The fluorescence intensity at 608 nm was measured in the presence of analytes, and the result is shown in Fig. 2B. All these representative interfering species such as H₂O₂, ¹O₂, ONOO⁻, OH˙, O₂⁻, Cys, GSH, Hcy, S²⁻, SO₃²⁻, HSO₃⁻, HSO₄⁻, SO₄²⁻, Br⁻, F⁻, Cl⁻, P₂O₇⁴⁻, PO₄³⁻, H₂PO₄⁻, OH⁻, CH₃COO⁻, HCO₃⁻, NO₃⁻ and NO₂⁻ lead to a negligible change in the fluorescence spectra of probe **DP** (Fig. S9†). In contrast, the addition of HOCl resulted in a significant enhancement of the fluorescence intensity of **DP** at around 608 nm. To further verify the utility of the probe, competition experiments were subsequently performed. The fluorescence intensity of probe **DP** towards HOCl in the presence of various competing analytes was recorded at 608 nm. As shown in Fig. 2B, **DP** exhibited a similar fluorescence response toward HOCl with the coexistence of other interfering species, indicating high specificity of **DP** for HOCl even in a complicated system. The selectivity of **DP** towards HOCl was also verified by the "naked-eye" fluorescence colorimetric assay. The colourless fluorescence turned red exclusively in the presence of HOCl (Fig. 2C). Due to the high selectivity of **DP** towards HOCl and observable color responses,

DP then serves as a potential indicator for HOCl detection in water samples. In the presence of increasing concentrations of HOCl from 0 to 60 µM, the solution of **DP** gradually changed from blue to yellowish-brown and the silent fluorescence color turned to red (Fig. S10†). Accordingly, **DP** can be used for the semi-quantitative analysis of the level of HOCl by "naked eye".

Considering the high reactivity of HOCl in live organisms, a fluorescent probe with fast response towards HOCl is highly desirable.[52] We then investigated time-profile fluorescence enhancement at 608 nm of probe **DP** in the presence of 0–50 µM HOCl. As shown in Fig. 2D, **DP** displayed quenching and stable fluorescence emission with excitation at 480 nm. In the presence of 20 µM HOCl, the emission of **DP** at 608 nm increased rapidly and reached a plateau within 30 s, and then maintained a steady level. In addition, a high concentration of HOCl took a longer time to achieve fluorescence intensity saturation. When 50 µM of HOCl was added, the emission of **DP** at 608 nm reached an intensity plateau within 120 s. Overall, the rapid response of **DP** toward HOCl enables the potential application in tracking HOCl in biological systems.

Spectroscopic responses of DP=O towards sulfur dioxide derivatives (SO_3^{2-}/HSO_3^-)

Then, the sensing performances of the HOCl-induced oxidation product (**DP=O**) towards SO_3^{2-}/HSO_3^- were investigated by spectroscopic titration in PBS aqueous solutions (DMF : H_2O = 1 : 9, v/v, 20 mM, pH = 7.4). Fig. 3A and B show the changes in the

Fig. 3 UV-vis absorption spectra of **DP=O** (10 µM) in the presence of different amounts of (A) HSO_3^- (0–60 µM) and (B) SO_3^{2-} (0–40 µM) in PBS aqueous solutions (DMF : H_2O = 1 : 9, v/v, 20 mM, pH = 7.4). Inset: colorimetric changes of **DP=O** (a) in the absence and (b) in the presence of HSO_3^- (60 µM) and SO_3^{2-} (40 µM). Absorbances of **DP=O** at 480 nm as a function of HSO_3^-/SO_3^{2-} concentrations. (C) UV-vis absorption spectra of **DP=O** (10 µM) in PBS aqueous solutions (DMF : H_2O = 1 : 9, v/v, 20 mM, pH = 7.4) in the presence of various analytes (60 µM). (D) Colorimetric changes of **DP=O** (10 µM) in the presence of various analytes (60 µM) in PBS aqueous solutions (DMF : H_2O = 1 : 9, v/v, 20 mM, pH = 7.4). (1) free **DP=O**. (2) HSO_3^-, (3) SO_3^{2-}, (4) F^-, (5) Cl^-, (6) $P_2O_7^{4-}$, (7) PO_4^{3-}, (8) $H_2PO_4^-$, (9) Cys, (10) GSH, (11) Hcy, (12) S^{2-}, (13) HSO_4^-, (14) SO_4^{2-}, (15) H_2O_2, (16) $^1O_2$, (17) OH^-, (18) CH_3COO^-, (19) HCO_3^-, (20) NO_3^-, (21) $ONOO^-$, (22) NO_2^-, (23) Br^-, (24) OH.

UV-visible spectra and solution colors. The main absorption band of **DP=O** at 480 nm gradually decreased in the presence of HSO_3^- and SO_3^{2-}, which was accompanied by a clear visual change in the color of the **DP=O** solution from yellowish-brown to colorless. The absorbance of **DP=O** at 480 nm decreased remarkably with incremental addition of SO_3^{2-} and HSO_3^- and then reached the plateaus with adding 30 µM HSO_3^- and 40 µM SO_3^{2-}.

The nucleophilic addition reaction of the C=C double bond of **DP=O** towards SO_3^{2-}/HSO_3^- takes on high specificity. The interferences deriving from various potential analytes including anions (HCO_3^-, Br^-, F^-, Cl^-, $P_2O_7^{4-}$, PO_4^{3-}, $H_2PO_4^-$, OH^-, CH_3COO^-, NO_3^-, $ONOO^-$, NO_2^-, HSO_4^-, and SO_4^{2-}), ROS (H_2O_2, $^1O_2$, and $ONOO^-$) and RSS (Cys, S^{2-}, SO_3^{2-}, and HSO_3^-) induced silent responses towards **DP=O**. Although GSH and Hcy caused a slight decline of the absorption compared to that of SO_3^{2-}/HSO_3^- (Fig. 3C), it is still enough to distinguish between SO_3^{2-}/HSO_3^- from the interferences. The specificity of **DP=O** towards SO_3^{2-}/HSO_3^- was further confirmed by a "naked-eye" colorimetric assay. The colors of the **DP=O** solution were changed exclusively after the addition of SO_3^{2-}/HSO_3^- (Fig. 3D). The results indicated that **DP=O** was specific towards SO_3^{2-}/HSO_3^- detection over other competitive species.

The specific responses of **DP=O** in the presence of increasing amounts of HSO_3^- and SO_3^{2-} were then investigated by fluorescence titration in PBS aqueous solutions. With an increase in the amount of HSO_3^- and SO_3^{2-} added to the solution of **DP=O**, the fluorescence emission peak centred at 608 nm gradually decreased. The fluorescence intensity remained constant and the red fluorescence colors completely quenched when over 5.0 eq. of HSO_3^- and 3.0 eq. of SO_3^{2-} were added (Fig. 4A(a and b), Fig. 4B(a and b)), respectively. The fluorescence quenching of **DP=O** could be attributed to the intercept of the conjugation system after the 1,4-addition reaction of the C=C double bond of **DP=O** with HSO_3^- and SO_3^{2-}.[53] The detection limits ($3\sigma/K$) of **DP=O** towards SO_3^{2-} and HSO_3^- were then calculated to be 70.8 nM and 65.1 nM according to the IUPAC standard (Fig. 4A(c) and B(c)).

To verify the specificity of **DP=O** toward HSO_3^- and SO_3^{2-}, the emission responses were carried out in the presence of various competitive species, such as F^-, Cl^-, $P_2O_7^{4-}$, PO_4^{3-}, $H_2PO_4^-$, Cys, GSH, Hcy, S^{2-}, HSO_4^-, SO_4^{2-}, H_2O_2, $^1O_2$, OH^-, CH_3COO^-, HCO_3^-, NO_3^-, $ONOO^-$, NO_2^- and Br^-. As shown in Fig. 4C, SO_3^{2-}/HSO_3^- elicited an obvious decrease in the fluorescence at 608 nm. However, other analytes induced negligible fluorescence changes except for slight quenching in the presence of Hcy and GSH. Furthermore, the strong red fluorescence emission exclusively quenched for the addition of HSO_3^- and SO_3^{2-} to the **DP=O** solution, and other competitive analytes caused unconspicuous changes in the fluorescence color (Fig. 4D). These results indicated the desired selectivity of **DP=O** towards HSO_3^- and SO_3^{2-} over other analytes. Then, the response kinetic profiles of **DP=O** towards HSO_3^- and SO_3^{2-} were investigated to verify its real-time performance. When different concentrations of HSO_3^- and SO_3^{2-} were added into the solution of **DP=O**, the fluorescence intensity at 608 nm significantly declined within 600 seconds for SO_3^{2-} and 200 seconds for HSO_3^- (Fig. S11†). The results indicated the fast response times
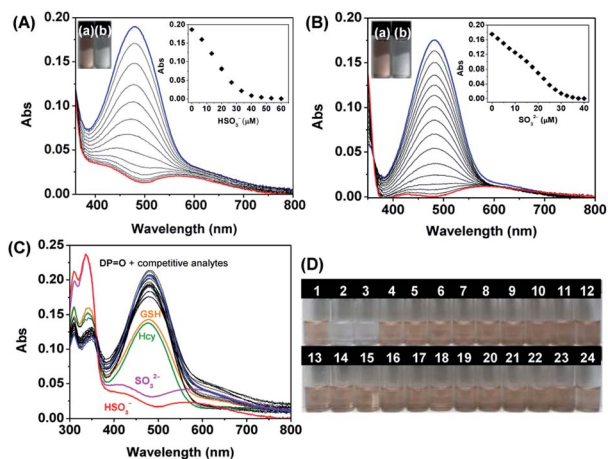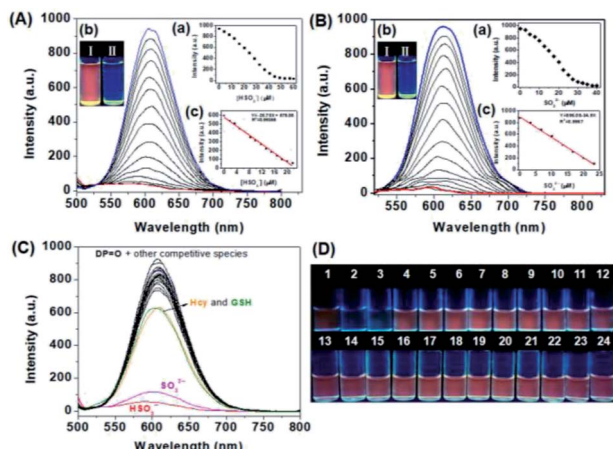
Fig. 4 (A) Fluorescence spectra of **DP=O** (10 μM) in the presence of different amounts of (A) HSO_3^- (0–60 μM) in PBS aqueous solutions (DMF : H_2O = 1 : 9, v/v, 20 mM, pH = 7.4). Inset: (a) fluorescence intensities of **DP=O** as a function of HSO_3^- concentrations. (b) Fluorescence color photos of **DP=O** (10 μM) in the presence of HSO_3^- (60 μM) under UV light. (c) Linear relationship between the fluorescence intensity of **DP=O** (5 μM) and HSO_3^- concentration (0–22 μM). (B) Fluorescence spectra of **DP=O** (10 μM) in the presence of different amounts of SO_3^{2-} (0–40 μM) in PBS aqueous solutions (DMF : H_2O = 1 : 9, v/v, 20 mM, pH = 7.4). Inset: (a) fluorescence intensities of **DP=O** as a function of SO_3^{2-} concentrations. (b) Fluorescence color photos of **DP=O** (10 μM) in the presence of SO_3^{2-} (40 μM) under UV light. (c) Linear relationship between the fluorescence intensity of **DP=O** (5 μM) and SO_3^{2-} concentration (0–23 μM). (C) Fluorescence spectra of **DP=O** (10 μM) in PBS aqueous solutions (DMF : H_2O = 1 : 9, v/v, 20 mM, pH = 7.4) in the presence of all kinds of analytes (60 μM). (D) Fluorescence color images of **DP=O** (10 μM) in the presence of various analytes (60 μM) under UV light in PBS aqueous solutions (DMF : H_2O = 1 : 9, v/v, 20 mM, pH = 7.4). (1) Free **DP=O**. (2) HSO_3^-, (3) SO_3^{2-}, (4) F^-, (5) Cl^-, (6) $P_2O_7^{4-}$, (7) PO_4^{3-}, (8) $H_2PO_4^-$, (9) Cys, (10) GSH, (11) Hcy, (12) S^{2-}, (13) HSO_4^-, (14) SO_4^{2-}, (15) H_2O_2, (16) $^1O_2$, (17) OH^-, (18) CH_3COO^-, (19) HCO_3^-, (20) NO_3^-, (21) $ONOO^-$, (22) NO_2^-, (23) Br^-, (24) OH. The intensities were recorded at 608 nm, and excitation was performed at 480 nm.

of **DP=O** toward HSO_3^- and SO_3^{2-} compared to those of the previously reported SO_2 derivative fluorescent probes.[54,55]

DP=O was also used for the semi-quantitative analysis of the levels of HSO_3^- and SO_3^{2-} in aqueous solutions by "naked eye" (Fig. S12†).

In addition, the responses of **DP** in the presence of HSO_3^- and SO_3^{2-} have also been measured and compared by spectroscopic titration. As shown in Fig. S13,† no remarkable responses of **DP** appeared in the presence of HSO_3^- and SO_3^{2-}, indicating the inert reaction of the C=C double bond with HSO_3^- and SO_3^{2-}. However, after the oxidation of the thioether of **DP** to a sulfoxide product (**DP=O**), the C=C double bond of **DP=O** was activated. Then, SO_3^{2-}/HSO_3^- reacts with **DP=O** via a 1,4-nucleophilic addition reaction mechanism leading to a decrease in the intensity of absorption and emission spectra (Fig. S14†).

Fluorescence imaging *in vitro* and *in vivo*

To verify the reliability of **DP** in the physiological pH range, the reactivity of **DP** towards HOCl and **DP=O** to $SO_3^{2-}/$

HSO_3^- under different pH values was tested. As shown in Fig. S15,† the fluorescence intensity of **DP** at 608 nm remained constant in the pH range of 5.8–8.0. Upon the addition of HOCl, the emission increased dramatically in the same pH range. Furthermore, the fluorescence responses of **DP=O** towards SO_3^-/HSO_3^{2-} were slightly affected in the pH range from 5.8 to 7.0 and reached a constant value over the pH range 7.0–8.0. The results indicated that **DP** could be used to sequentially detect HOCl and SO_3^-/HSO_3^{2-} in the physiological pH range. Then, the cytotoxicity of **DP** was measured by an MTT assay using a HeLa cell line.[56] It was found that 89% of HeLa cells were still alive after incubation with up to 10 μM **DP** for 24 h and the HeLa cell viability was still greater than 82.4% at a higher concentration of **DP** (30 μM) after 24 h of incubation (Fig. S16†), suggesting the low cytotoxicity of **DP**.

Encouraged by the outstanding performances of **DP** under simulated physiological conditions, we then explored the capabilities of **DP** to image HOCl and SO_3^{2-}/HSO_3^- in live cells. The application of **DP** in the sequential fluorescence imaging of HOCl and SO_3^{2-}/HSO_3^- *in vitro* was evaluated with live HeLa cells. As shown in Fig. 5a, the HeLa cells incubated with **DP** at 37 °C for 20 min present silent intracellular fluorescence. However, upon addition of HOCl and culturing for 25 min, the red fluorescence signal emerged significantly (Fig. 5d). The results indicated that **DP** is cell-permeable and capable of monitoring HOCl in live cells. In addition, when SO_3^{2-}/HSO_3^- was added to the above stained cells for further 30 min, the red fluorescence was quenched again (Fig. 5g), indicating the formation of the addition product **DP=O–SO$_3$** in live cells.
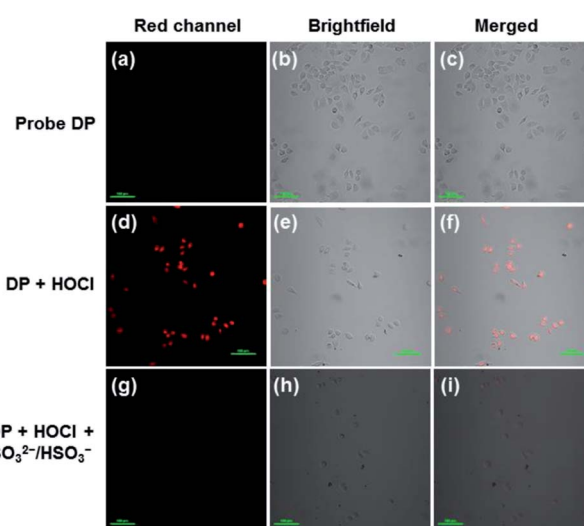

Fig. 5 Sequential fluorescence imaging of HOCl and SO_3^{2-}/HSO_3^- in live HeLa cells. (a–c) HeLa cells treated with **DP** (2 μM) for 20 min. (d–f) HeLa cells pre-treated with HOCl (10 μM) and then incubated with **DP** (2 μM) for further 25 min. (g–i) A549 cells pre-treated with HOCl (10 μM) and then incubated with **DP** (2 μM) for 25 min, and finally incubated with SO_3^{2-}/HSO_3^- (10 μM) for further 30 min. The images were acquired using a confocal microscope at 465 nm excitation and 610 nm emission. Scale bar = 100 μm.

Then, fluorescence imaging of HOCl and SO_3^{2-}/HSO_3^- *in vivo* was investigated in adult zebrafish and nude mice. Endogenous HOCl was generated in zebrafish by stimulation with lipopolysaccharides (LPS). Free zebrafish and LPS-stimulated zebrafish were used as the control groups. As shown in Fig. S17,† no fluorescence was observed in the control groups. However, intense red fluorescence on the gill and abdomen in zebrafish gradually increased over time when the LPS-stimulated zebrafish was further stained with **DP**. The results indicated that LPS stimulation-generated HOCl reacted with **DP** to generate the oxidized product (**DP=O**) in live zebrafish. Furthermore, after the **DP=O** loaded zebrafish were sequentially stimulated with SO_3^{2-}/HSO_3^-, the red fluorescence signal in zebrafish was then quenched over time (Fig. S18 and S19†), which demonstrated the occurrence of the addition reaction of **DP=O** with SO_3^{2-} and HSO_3^-.

It has been reported that long–emission wavelength light has advantages including minimum photodamage, deep penetration into tissues, and low interference from autofluorescence. Due to the long emission wavelength (608 nm) of **DP**, the capability of **DP** for the sequential visualization of HOCl and SO_3^{2-}/HSO_3^- *in vivo* was further verified in live nude mice (6–8 week). **DP** was subcutaneously injected into the hind limbs of 6–8 week-old nude mice, followed by the sequential treatment of HOCl and SO_3^{2-}/HSO_3^- in the same area. Fluorescence imaging was then performed at different time courses after the administration. As shown in Fig. 6, the free mouse and **DP**-injected mice showed no fluorescence signal. By contrast, an intense fluorescence signal was noted over time after the mouse was treated with HOCl.

Then, the *in situ* produced **DP=O** can be employed as an imaging agent for visualizing SO_3^{2-}/HSO_3^- *in vivo*. As shown in Fig. 7, the right hind limbs of mice displayed a robust fluorescence signal compared with the control group after **DP=O** was *in situ* generated in the injected area. Then, the fluorescence signal decreased gradually until it vanished when SO_3^{2-}/HSO_3^- was subcutaneously injected into the same areas. The fluorescence imaging studies in adult zebrafish and nude mouse adequately indicated that **DP** can be used as an effective tool for the sequential monitoring of HOCl and SO_3^{2-}/HSO_3^- *in vivo*.
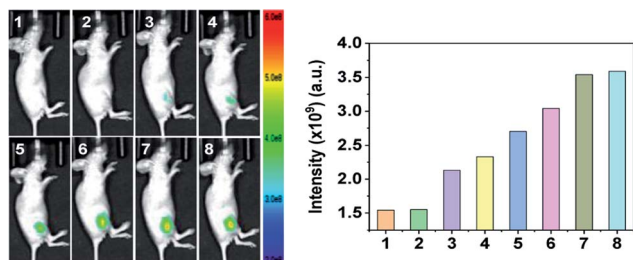

Fig. 6 Fluorescence imaging of exogenous HOCl in live mice. (1) Nude mouse; (2) DP (20 μM, 125 μL) was subcutaneously injected into the mouse; (3) followed by the injection of 25 μL HOCl (0.1 mM) to this area. Images were then recorded at different time points: (4) 5 min, (5) 10 min, (6) 15 min, (7) 20 min and (8) 25 min. The mouse was imaged using an excitation filter (465 nm) and an emission filter (610 nm).
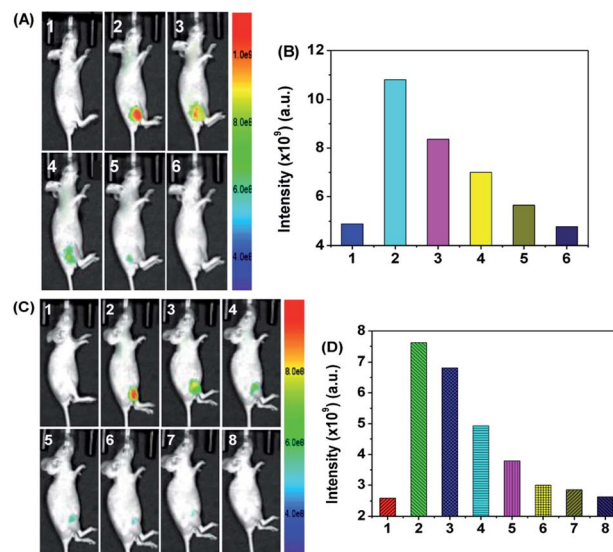

Fig. 7 Fluorescence imaging SO_3^{2-}/HSO_3^- intake in mice. (A) (1) Control group; (2) 20 μM (125 μL) DP=O was subcutaneously injected into the left hind limbs of the mouse; then SO_3^{2-} (0.1 mM) was injected into the same areas of interest: (3) 5 min, (4) 10 min, (5) 15 min, (6) 20 min, (7) 25 min and (8) 30 min post injection. (C) (1) Control group; (2) 20 μM (125 μL) DP=O was subcutaneously injected into the left hind limbs of the mouse; then HSO_3^- (0.1 mM) was injected into the same areas of interest for (3) 5 min, (4) 10 min, (5) 20 min and (6) 30 min post injection. (B) and (D) Mean fluorescence intensity of interested areas at different time points shown in (A) and (C). The mice were imaged with an excitation filter at 465 nm and an emission filter at 610 nm.

Experimental

Synthesis of the fluorescent probe DP

2-[3-Cyano-4,5,5-trimethylfuran-2(5H)-ylidene]malononitrile (DCDHF)[57] (0.199 g, 1 mmol) and 10-ethyl-10H-phenothiazine-3-carbaldehyde[58] (0.269 g, 1 mmol) were dissolved in hot ethanol, respectively. Then, the two solutions were mixed and two drops of piperidine were added. The reaction mixture was refluxed for 6 hours in an argon atmosphere. The precipitate was filtrated, washed with cold ethanol and dried under vacuum. The crude product was further purified by recrystallization in acetonitrile to get the purple-black solid **DP** with 65% yield. ^{1}H-NMR (600 MHz, DMSO-d_6) δ (ppm): 7.76–7.91 (Ar–H, 3H), 7.06–7.28 (Ar–H and C=C–H, 6H), 3.97 (–CH_2, 2H), 1.68–1.83 (–CH_3 and –CH_2, 8H), 1.01 (CH_3, 3H). ^{13}C NMR (151 MHz, $CDCl_3$): 177.7, 175.8, 148.9, 147.1, 143.3, 131.3, 129.1, 128.4, 128.0, 127.7, 124.1, 122.7, 117.0, 116.3, 113.4, 113.3, 112.6, 111.7, 99.5, 97.5, 53.9, 49.1, 25.7, 19.9, 11.3. HRMS-API (positive mode, m/z) for [**DP+H**]$^+$: calcd 451.15926, found: 451.15936. Mp: 184.4–185.2 °C.

General procedures of spectra detection

Stock solutions of **DP** were prepared at 0.5 mM in DMF, and the solution of **DP** was diluted with a PBS solution to 10 μM (DMF : H_2O = 1 : 9, v/v, 20 mM, pH = 7.4). The ROS species were prepared in water according to the procedure previously

reported in the literature.[59] The solutions of various testing analytes (20 mM) were prepared in distilled water. For spectroscopic response of **DP** to HOCl and **DP=O** to SO_3^{2-}/HSO_3^-, HOCl and SO_3^{2-}/HSO_3^- at different concentrations were added into the probe solution (total volume: 3 mL), followed by immediate spectroscopic measurements. Excitation and emission slits are 5 nm, respectively.

Confocal fluorescence imaging in HeLa cells

Confocal fluorescence imaging was carried out at the School of Forensic Medicine, Xinxiang Medical University. For the visualisation of exogenous HOCl in live HeLa cells, HeLa cells were seeded at a density of 1.5×10^5 cells per mL in 22 mm coverglass bottom culture dishes. After replacement of the culture medium, the cells were incubated with fresh PBS containing **DP** (2 μM). After 20 min incubation, the cells were sequentially treated with 10 μM HOCl and SO_3^{2-}/HSO_3^- (10 μM) for further 25 min, respectively. The cells were washed three times with PBS to remove excess analytes and then subjected to confocal microscope fluorescence imaging. All the A549 cells were imaged using an excitation filter (465 nm) and an emission filter (610 nm). Scale bar = 100 μm.

Fluorescence imaging of endogenous HOCl generation in adult zebrafish[60]

Adult zebrafish was stimulated with LPS (2 μL mL^{-1}) for 3 h, and then stained with **DP** (10 μM) for 5 min, 10 min and 15 min, respectively. Blank zebrafish was chosen as the control group. Zebrafish was imaged with an excitation filter (465 nm) and an emission filter (610 nm).

Fluorescence imaging of SO_3^{2-}/HSO_3^- in adult zebrafish

DP=O (10 μM) was prepared by addition of 5 equiv. HOCl into a PBS aqueous solution (DMF : H$_2$O = 1 : 9, v/v, 20 mM, pH = 7.4). Adult zebrafish was first stimulated with **DP=O** (10 μM) for 30 min, and then stained with SO_3^{2-} (40 μM) and HSO_3^- (40 μM) for 5 min, 10 min, 15 min, 20 min, 25 min, 30 min, 35 min and 40 min, respectively. Zebrafish were imaged with an excitation filter (465 nm) and an emission filter (610 nm).

Fluorescence imaging of exogenous HOCl in live mice

Nude mice (6–8 week old mice) were anesthetized with isoflurane in a flow of oxygen throughout the experiments. For imaging of exogenous HOCl in live mice, **DP** (20 μM, 125 μL) was subcutaneously injected into mice, followed by the injection of 25 μL (0.1 mM) HOCl in the same area. Imaging for the injection area was performed every 5 min within 25 min with an excitation filter at 465 nm and an emission filter at 610 nm.

Fluorescence visualization of SO_3^{2-} and HSO_3^- intake in mice

Nude mice were anesthetized with isoflurane in a flow of oxygen. **DP=O** (10 μM) was prepared by addition of 5 equiv. HOCl into a PBS aqueous solution (DMF : H$_2$O = 1 : 9, v/v, 20 mM, pH = 7.4). For the imaging of exogenous SO_3^{2-} and HSO_3^- in live mice, **DP=O** (20 μM 125 μL) was subcutaneously

injected into the right hind limbs of the mouse; then SO_3^{2-} (0.1 mM) and HSO_3^- (0.1 mM) were injected into the same areas of interest. Imaging for the injection area was performed every 5 min within 30 min with an excitation filter at 465 nm and an emission filter at 610 nm.

Conclusions

In summary, we have successfully developed a red-emitting fluorescent probe (**DP**) for the sequential detection of hypochlorous acid (HOCl) and sulfur dioxide derivatives (SO_3^{2-}/HSO_3^-) *in vitro* and *in vivo*. **DP** possesses a donor–π–acceptor (D–π–A) structure, in which the phenothiazine unit acts as the electron-donating group (EDG), while DCDHF acts as the electron-withdrawing group (EWG). The thioether moiety of **DP** can be exclusively oxidized to sulfoxide (**DP=O**) in the presence of HOCl, resulting in the hypochromic shift of the absorption spectra and "OFF–ON" response of the emission. Furthermore, after the activation of the C=C double bond by oxidation, **DP=O** reacts with SO_3^{2-}/HSO_3^- *via* a nucleophilic addition reaction leading to a decrease in the intensity of absorption and emission spectra, which enabled the realization of sequential detection of HOCl and SO_3^{2-}/HSO_3^- by a single fluorescent probe. The proposed reaction mechanisms of **DP** towards HOCl and SO_3^{2-}/HSO_3^- have been confirmed by spectroscopic titration and high-resolution mass spectroscopy (HRMS). **DP** has the advantages of high water solubility, reliability in the physiological pH range, red-emission, outstanding selectivity and low cytotoxicity, which enabled its practical values in biological fields. **DP**'s application in biological systems was demonstrated by the monitoring of HOCl and SO_3^{2-}/HSO_3^- in live cells and live animal models. The successful applications of the fluorescent probe prove that it would be a useful tool for the detection and monitoring of the redox equilibrium regulation–related bioactive species in living systems.

Ethical statement

All animal procedures were performed in accordance with the Guidelines for the Care and Use of Laboratory Animals of Dalian Medical University and experiments were approved by the Animal Ethics Committee of the University of Science and Technology Liaoning.

Author contributions

Q. T. Meng and Z. Q. Zhang designed and guided the study, analyzed all the data and wrote the manuscript. J. H. Liu, H. Y. Yin and Z. Y. Shang performed the synthesis, spectroscopic titration measurements and data processing. P. Gu and G. J. He performed the fluorescence microscopy imaging in live cells. R. Zhang contributed to review and polish the manuscript. All authors have read and agreed to the published version of the manuscript.

Conflicts of interest

There are no conflicts to declare.

Acknowledgements

References

1 Y. Zhang, Y. Zuo, T. Yang, Z. Gou, X. Wang and W. Lin, *Analyst*, 2019, **144**, 5075–5080.

2 Y. Cui, Z. Lu, L. Bai, Z. Shi, W. Zhao and B. Zhao, *Eur. J. Cancer*, 2007, **43**, 2590–2601.

3 M. Valko, D. Leibfritz, J. Moncol, M. T. D. Cronin, M. Mazur and J. Telser, *Int. J. Biochem. Cell Biol.*, 2007, **39**, 44–84.

4 A. J. Kettle and C. C. Winterbourn, *Redox Rep.*, 1997, **3**, 3–15.

5 D. Roos and C. C. Winterbourn, *Science*, 2002, **296**, 669–671.

6 B. C. Dickinson and C. J. Chang, *Nat. Chem. Biol.*, 2011, **7**, 504–511.

7 X. Lv, X. Yuan, Y. Wang and W. Guo, *New J. Chem.*, 2018, **42**, 15105–15110.

8 T. Finkel and N. J. Holbrook, *Nature*, 2000, **40**, 239–247.

9 H. Li, Z. Cao, D. R. Moore, P. L Jackson, S. Barnes, J. D. Lambeth, V. J. Thannickal and G. Cheng, *Infect. Immun.*, 2012, **80**, 2528–2537.

10 Z. Lou, P. Li, Q. Pan and K. Han, *Chem. Commun.*, 2013, **49**, 2445–2447.

11 A. Daugherty, J. L. Dunn, D. L Rateri and J. W. Heinecke, *J. Clin. Invest.*, 1994, **94**, 437–444.

12 S. Hammerschmidt, N. Büchler and H. Wahn, *Chest*, 2002, **121**, 573–581.

13 Y. W. Yap, M. Whiteman and N. S. Cheung, *Cell. Signalling*, 2007, **19**, 219–228.

14 M. J. Steinbeck, L. J. Nesti, P. F. Sharkey and J. Parvizi, *J. Orthop. Res.*, 2007, **25**, 1128–1135.

15 E. A. Podrez, H. M. Abu-Soud and S. L. Hazen, *Free Radical Biol. Med.*, 2000, **28**, 1717–1725.

16 Z. Lou, P. Li and K. Han, *Acc. Chem. Res.*, 2015, **48**, 1358–1368.

17 Z. Lou, P. Li, Q. Pan and K. Han, *Chem. Commun.*, 2013, **49**, 2445–2447.

18 M. Valko, D. Leibfritz, J. Moncol, M. T. D. Cronin, M. Mazur and J. Telser, *Int. J. Biochem. Cell Biol.*, 2007, **39**, 44–84.

19 J. Nordberg and E. S. J. Arner, *Free Radicals Biol. Med.*, 2001, **31**, 1287–1312.

20 J.-Z. Li, Y.-H. Sun, C.-Y. Wang, Z.-Q. Guo, Y.-J. Shen and W.-H. Zhu, *Anal. Chem.*, 2019, **91**, 11946–11951.

21 M. H. Stipanuk and I. J. Ueki, *Inherited Metab. Dis.*, 2011, **34**, 17–32.

22 Q. Z. Meng, G. Qin, B. Zhang and J. L. Bai, *Mutagenesis*, 2004, **19**, 465–468.

23 X. Shi, *J. Inorg. Biochem.*, 1994, **56**, 155–165.

24 Y. Ma, Y. Tang, Y. Zhao and W. Lin, *Anal. Chem.*, 2019, **91**, 10723–10730.

25 X. B. Wang, H. F. Jin, C. S. Tang and J. B. Du, *Clin. Exp. Pharmacol. Physiol.*, 2010, **37**, 745–752.

26 N. Sang, Y. Yun, H. Li, L. Hou, M. Han and G. Li, *Toxicol. Sci.*, 2010, **114**, 226–236.

27 G. Chen, W. Zhou, C. Zhao, Y. Liu, T. Chen, Y. Li and B. Tang, *Anal. Chem.*, 2018, **90**, 12442–12448.

28 B. Li, M. J. Chen, L. Guo, Y. Yun, G. K. Li and N. Sang, *Toxicol. Sci.*, 2015, **147**, 535–548.

29 H. Agarwalla, S. Pal, A. Paul, Y. W. Jun, J. Bae, K. H. Ahn, D. N. Srivastava and A. Das, *J. Mater. Chem. B*, 2016, **4**, 7888–7894.

30 Z. Du and Z. Meng, *Food Chem. Toxicol.*, 2004, **42**, 1211–1216.

31 H. Vally, N. L. Misso and V. Madan, *Clin. Exp. Allergy*, 2009, **39**, 1643–1651.

32 W. J. FAO in *WHO food additives series*, World Health Organization, Geneva, 60th edn, 2009.

33 M. Gao, X. Zhang, Y. Wang, Q. Liu, F. Yu, Y. Huang, C. Ding and L. Chen, *Anal. Chem.*, 2019, **91**, 7774–7781.

34 J. Ren, P. Zhang, H. Liu, C. Zhang, Y. Gao, J. Cui and J. Chen, *Sens. Actuators, B*, 2020, **304**, 127299.

35 R. Zhang and J. Yuan, *Acc. Chem. Res.*, 2020, **53**, 1316–13297.

36 S. Ma, G. Chen, J. Xu, Y. Liu, G. Li, T. Chen, Y. Li and T. D. James, *Coord. Chem. Rev.*, 2021, **427**, 213553.

37 H. Feng, Q. Meng, Y. Wang, C. Duan, C. Wang, H. Jia, Z. Zhang and R. Zhang, *Chem.–Asian J.*, 2018, **13**, 2611–2618.

38 H. Feng, Z. Zhang, Q. Meng, H. Jia, Y. Wang and R. Zhang, *Adv. Sci.*, 2018, **5**, 1800397.

39 H. Jia, S. Xia, H. Feng, Q. Meng, C. Duan, Z. Zhang and R. Zhang, *Org. Biomol. Chem.*, 2018, **16**, 2074–2082.

40 H. Feng, Y. Wang, J. Liu, Z. Zhang, X. Yang, R. Chen, Q. Meng and R. Zhang, *J. Mater. Chem. B*, 2019, **7**, 3909–3916.

41 F. Zhou, H. Feng, H. Li, Y. Wang, Z. Zhang, W. Kang, H. Jia, X. Yang, Q. Meng and R. Zhang, *ACS Omega*, 2020, **5**, 5452–5459.

42 F. Zhou, Y. Sultanbawa, H. Feng, Y.-L. Wang, Q. Meng, Y. Wang, Z. Zhang and R. Zhang, *J. Agric. Food Chem.*, 2019, **67**, 4375–4383.

43 X. Yang, Y. Wang, Z. Shang, Z. Zhang, H. Chi, Z. Zhang, R. Zhang and Q. Meng, *RSC Adv.*, 2021, **11**, 31656–33166.

44 K. Li, S. Xu, M. Xiong, S.-Y. Huan, L. Yuan and X.-B. Zhang, *Chem. Soc. Rev.*, 2021, **50**, 11766–11784.

45 K. H. Kim, S. J. Kim, S. Singha, Y. J. Yang, S. K. Park and K. H. Ahn, *ACS Sens.*, 2021, **6**, 3253–3261.

46 H. Li, Q. Yao, J. Fan, C. Hu, F. Xu, J. Du, J. Wang and X. Peng, *Ind. Eng. Chem. Res.*, 2016, **55**, 1477–1483.

47 J. Han, S. Yang, B. Wang and X. Song, *Anal. Chem.*, 2021, **93**(12), 5194–5200.

48 K. Dou, G. Chen, F. Yu, Z. Sun, G. Li, X. Zhao, L. Chen and J. You, *J. Mater. Chem. B*, 2017, **5**, 8389–8398.

49 Y. K. Yue, F. J. Huo, C. X. Yin, J. B. Chao, Y. B. Zhang and X. Wei, *RSC Adv.*, 2015, **5**, 77670–77672.

50 L. Y. Zhou, D. Q. Lu, Q. Q. Wang, S. H. Liu, Q. L. Lin and H. Y. Sun, *Biosens. Bioelectron.*, 2017, **91**, 699–705.

51 S. T. Cai, C. Liu, X. J. Jiao, L. C. Zhao and X. S. Zeng, *J. Mater. Chem. B*, 2020, **8**, 2269–2274.

52 P. Zhang, H. Wang, Y. Hong, M. Yu, R. Zeng, Y. Long and J. Chen, *Biosens. Bioelectron.*, 2018, **99**, 318–324.

53 G. Yuan, L. Zhou, Q. Yang, H. Ding, L. Tan and L. Peng, *J. Agric. Food Chem.*, 2021, **69**, 4894–4902.

54 J. Wang, Y. Hao, H. Wang, S. Yang, H. Tian, B. Sun and Y. Liu, *J. Agric. Food Chem.*, 2017, **65**, 2883–2887.

55 W. Xu, O. L. Teoh, J. J. Peng, D. D. Su, L. Yuan and Y. T. Chang, *Biomaterials*, 2015, **56**, 1–9.

56 L. Yang, Y. Zhang, X. Ren, B. Wang, Z. Yang, X. Song and W. Wang, *Anal. Chem.*, 2020, **92**, 4387–4394.

57 J. Park, H. Kim, Y. Choi and Y. Kim, *Analyst*, 2013, **138**, 3368–3371.

58 H. Xiao, K. Xin, H. Dou, G. Yin, Y. Quan and R. Wang, *Chem. Commun.*, 2015, **51**, 1442–1445.

59 J. J. Hu, N.-K. Wong, S. Ye, X. Chen, M.-Y. Lu, A. Q. Zhao, Y. Guo, A. C.-H. Ma, A. Y.-H. Leung, J. Shen and D. Yang, *J. Am. Chem. Soc.*, 2015, **137**, 6837–6843.

60 H. Fang, R. A. Pengal, X. Cao, L. P. Ganesan, M. D. Wewers, C. B. Marsh and S. Tridandapani, *J. Immunol.*, 2004, **173**, 360–366.